Constraining the equation of state of supra-nuclear dense matter from XMM-Newton observations of neutron stars in globular clusters

Natalie A. Webb [1] and Didier Barret[1]
Centre d'Etude Spatiale des Rayonnements, 9 Avenue du Colonel Roche, 31028 Toulouse Cedex 04, France
Natalie.Webb@cesr.fr

ABSTRACT

We report on the detailed modelling of the X-ray spectra of three likely neutron stars. The neutron stars, observed with XMM-Newton are found in three quiescent X-ray binaries in the globular clusters: ω Cen, M 13 and NGC 2808. Whether they are accreting at very low rates or radiating energy from an accretion heated core, their X-ray spectra are expected to be those of a hydrogen atmosphere. We use and compare publicly available hydrogen atmosphere models, with constant and varying surface gravities to constrain the masses and radii of the neutron stars. Thanks to the high XMM-Newton throughput, and the accurate distances available for these clusters, using the latest science analysis software release and calibration of the XMM-Newton EPIC cameras, we derive the most stringent constraints on the masses and radii of the neutron stars obtained to date from these systems. A comparison of the models indicate that previously used hydrogen atmosphere models (assuming constant surface gravity) tend to underestimate the mass and overestimate the radius of neutron stars. Our data constrain the allowed equations of state to those which concern normal nucleonic matter and one possible strange quark matter model, thus constraining radii to be from 8 km and masses up to 2.4 $M_{\odot}$.

Subject headings: Stars: neutron — Dense matter — Equation of state — globular clusters: individual(ω Cen, M 13, NGC 2808) — X-rays: stars

1. Introduction

Forty years after their discovery, the nature of the material making up the core of neutron stars remains largely unknown. At densities above a few times the equilibrium density of nuclear matter, models predict the existence of exotic components such as pion or kaon condensates or unconfined quarks (e.g. Lattimer & Prakash 2007). The exciting idea that neutron stars may contain exotic forms of matter makes them of prime interest, not only for astrophysics but for physics in general.

Different equations of state of dense matter predict different maximum masses and different mass-radius relationships. So far accurate mass measurements have been made for radio pulsars giving masses ranging from $1.18\pm^{0.03}_{0.02}$ $M_{\odot}$, for the case of one of the pulsars in PSR J1756-2251 (Faulkner et al. 2005) to 1.4414±0.0002 $M_{\odot}$, for PSR B1913+16 (Weisberg & Taylor 2005). Such low values can be accommodated by a wide range of equations of states and do not provide a strong constraint on the composition of dense matter. There is however growing evidence that neutron stars, as massive as 2 $M_{\odot}$, may also exist, in particular in accreting X-ray binaries, as inferred from the study of the properties of kilo-Hz QPOs (Quasi-Periodic Oscillations) (e.g. the neutron star in 4U 1636-536 which is estimated to have a mass of 1.9-2.1 $M_{\odot}$ Barret, Olive & Miller (2005)) and binary millisecond pulsars that are no longer accreting (e.g. PSR J0751+1807, which has a mass measured through relativistic orbital decay of 2.1±0.2 $M_{\odot}$, Nice et al. 2005). If the latter estimates are confirmed (by dynamical mass estimates of the binary components), they would rule

out some exotic forms of matter, such as quarks or pion condensates.

While there are some accurate mass measurements already available, the situation is different with radii which are much harder to constrain. X-ray spectroscopy is one promising avenue to follow to tackle this issue. So far, there has been one single (and still debated) measurement of redshifted absorption lines in the combined early and late type I X-ray burst spectra of the X-ray binary EXO 0748-676. The line energies are consistent with FeXXVI Hα (n = 2-3) and FeXXV Heα (n = 2-3), respectively, both at the same redshift z = 0.350±0.005 (Cottam, Paerels & Mendez 2002). The measured redshift provided a direct estimate of Mass/Radius (M/R) ($M/R = \frac{c^2}{2G}(1 - (1+z)^{-2})$. Assuming a canonical mass of 1.4 $M_\odot$, this would imply a radius of about 9 km. Following this result, and using the burst properties, Özel (2006) estimated both mass and radius separately. This led to a massive neutron star with a mass $M \geq 2.10 \pm 0.28 M_\odot$ (and $R \geq 13.8 \pm 1.8$ km) in EXO 0748-676, a result suggesting again that if this system is typical, exotic forms of matter, such as condensates and unconfined quarks do not exist in neutron star cores.

Another promising way of inferring radii is through observations of quiescent X-ray emission from neutron stars for which the distance (d) can be estimated reliably ($F_\infty = (R_\infty/d)^2 \sigma T_\infty^4$, where F_∞, T_∞ are the flux and radiation temperatures redshifted to the Earth and $R_\infty = R/\sqrt{1-2GM/Rc^2}$ is the radiation radius). Whether the energy reservoir is the heat deposited deep in the neutron star crust during the outburst phase of the transient (Brown, Bildsten & Rutledge 1998), or sustained by a low-level of radial accretion (Van Paradijs et al. 1987) (via an advection dominated accretion flow), the X-rays originate from the atmosphere of the neutron star. The spectrum radiated by the atmosphere will depend on its actual composition, the strength and the structure of the magnetic field. In general, it is thought that the old neutron stars in globular clusters have low magnetic fields and hydrogen-rich atmospheres (gravitational settling of heavier elements occurs rapidly, see Rutledge et al. (2002) and references therein). Early non magnetic hydrogen atmosphere models have been shown to provide adequate fits to the quiescent X-ray spectra of several neutron star systems, all providing plausible values for the neutron star radius (typically around 10 km, Rutledge et al. 2002; Gendre et al. 2003a,b). Compared to neutron stars in the field, those in globular clusters have accurate distance estimates, and the fitting of their very soft spectra is made easier by the fact that at least the value of the interstellar absorption derived from the optical extinction is well known, even if the absorption intrinsic to the system is largely unknown.

Following the work done by Heinke et al. (2006) on Chandra data of the quiescent neutron star X-ray binary X7 in 47 Tucanae, we apply recently improved neutron star atmosphere models, available in the latest release of the XSPEC spectral fitting package (version 12.3.0, Arnaud 1996), to three neutron stars in quiescent X-ray binaries that we have observed in three globular clusters with XMM-Newton. This is part of an on-going program to locate, identify and classify faint X-ray sources in globular clusters (Servillat et al. 2007; Gendre et al. 2003a,b; Webb et al. 2004, 2006), with an aim to determining the internal energy source that slows down the inevitable collapse of globular clusters. Early fitting of the X-ray spectra with the first hydrogen-atmosphere models of Zavlin, Pavlov, & Shibanov (1996) assuming a constant surface gravity ($\log g_s$=14.385, corresponding to a 1.4 $M_\odot$ and 10 km radius neutron star), were reported for ω Cen and M 13 in Gendre et al. (2003a,b). However, as emphasised by Heinke et al. (2006), using models with appropriate surface gravity for each fitted value of the mass and radius of the neutron star is important when interpreting high quality X-ray spectra, which is indeed the case for the spectra measured with XMM-Newton. Applying the improved models is the main motivation of this paper, which further benefits from improved data analysis software and calibration of the EPIC instruments compared to the earlier published results on these sources.

In the next section, we describe the observations, recalling the essential parameters of the clusters (distance, extinction,...), the data reduction and present the results of the spectral fitting. We use, for comparison purposes three different models, described hereafter.

2. Observations and data reduction

We have observations of the three likely neutron stars in three different globular clusters, ω Centauri (ω Cen), M 13 and NGC 2808. Observations of each of these clusters were made with the X-ray observatory XMM-Newton. All three EPIC cameras were used in the full-frame mode with the medium filter. Further information about these observations can be found in Table 1.

To reduce these data we used the latest version of the XMM-Newton Science Analysis Software (SAS, version 7.0). This has many improvements over the earlier versions of the SAS used to reduce ω Cen and M 13 (version 5.3.3) such as upgraded EPIC calibration, resulting in a much better cross calibration among the EPIC instruments and which includes modelling of spatial and temporal response dependencies. Improvements to the bad pixel finding algorithms (decreasing the noise at low energies significantly, important for neutron stars which emit mainly at low energies), the vignetting correction and exposure maps have also been made (see the SAS release notes[1]). The MOS data were reduced using the 'emchain'. The event lists were filtered, so that 0-12 of the predefined patterns (single, double, triple, and quadruple pixel events) were retained and the high background periods were identified by defining a count rate threshold above the low background rate and the periods of soft proton flares were then flagged in the event list. We also filtered in energy. We used the energy range 0.2-10.0 keV, as recommended in the document 'EPIC Status of Calibration and Data Analysis' (Kirsch et al. 2002). The *pn* data were reduced using the 'epchain' of the SAS. Again the event lists were filtered, so that 0-4 of the predefined patterns (single and double events) were retained, as these have the best energy calibration. We again filtered in energy, where we used the energy range 0.2-10.0 keV and we also filtered for the soft proton flares. A summary of the observations and good time intervals for each observation and camera is given in Table 1.

We extracted the ω Cen spectra using circles of radii $\sim 45''$ (to include at least 90% of the available flux from the neutron star) centred on the source. For the neutron star in M 13 we used an extraction radius of $\sim 25''$ due its close proximity to other sources and excluded a region of radius $15''$ around a second source that fell in the extraction region (the large region contains at least 80% of the total source counts from the neutron star and less than 10% of the counts from the neighbouring source, Ehle et al. (2006)), see Fig 1. Due to over-crowding in the centre of NGC 2808 we used extraction regions of $8''$, which includes 50% of the total source counts from the neutron star (Ehle et al. 2006), see Fig 2. We used a similar neighbouring region, free from X-ray sources to extract a background spectrum. We rebinned the MOS data into 15 eV bins and the *pn* data into 5eV bins as recommended in Ehle et al. (2006). We used the SAS tasks 'rmfgen' and 'arfgen' to generate a 'redistribution matrix file' and an 'ancillary response file', for each spectrum.

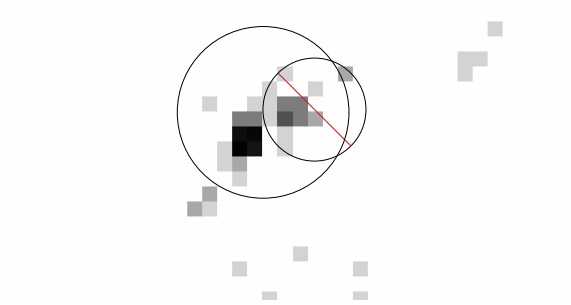

Fig. 1.— Image showing the region used to extract the M 13 neutron star spectrum (brighter source) and the region excluded due to the source found at $18.4''$ from the neutron star, superposed on the MOS 1 data (0.2-10.0 keV).

3. Spectral Analysis

We exploit three different hydrogen atmosphere models that are publicly available in Xspec 12.3.0. These are the basic neutron star atmosphere model (nsa) that we used previously in Gendre et al. (2003a,b). This model includes a uniform surface (effective) temperature, either a non-magnetised neutron star or with a field B = 10^{12} or B = 10^{13} G and a radiative atmosphere in hydrostatic equilibrium. The nsagrav model used is similar, but allows for a variety of surface gravitational accelerations, ranging from 10^{13}

[1] http://xmm.vilspa.esa.es/sas/7.0.0/documentation/releasenotes/

Table 1: Summary of the globular clusters (GC) and their observations.

GC	Date	Det.	T_{obs}	GTI	Dist.	n_H
ω Cen	2001 Aug 13	M1	40	40	5.3	0.067
		M2	40	40		
		pn	40	40		
M 13	2002 Jan 28	M1	17	12	7.7	0.011
		M2	17	11		
		pn	14	8		
M 13	2002 Jan 30	M1	18	14		
		M2	18	14		
		pn	13	8		
M 13	1990 Jun 1	PSPC	46	46		
NGC 2808	2005 Feb 2	M1	41	41	9.6	0.128
		M2	41	41		
		pn	40	31		

Det. indicates the detector used (M1/M2= MOS 1 or 2), T_{obs} gives the observation time in ks and GTI gives the good timing interval (in ks) after filtering for soft proton flares. The distances (Dist.) are taken from Harris (1999) and are given in kpc. The column densities (n_H, $\times 10^{22}$ cm^{-2}) to these clusters are from Harris (1999); Predehl & Schmitt (1995).

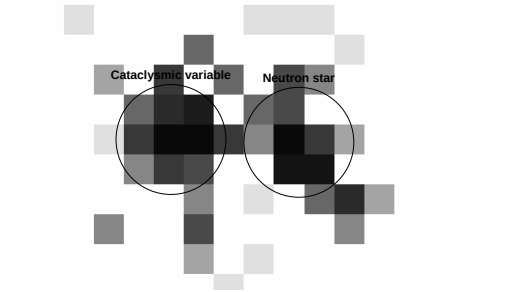

Fig. 2.— MOS 1 image (0.2-10.0 keV) showing the region used to extract the NGC 2808 neutron star spectrum and it's proximity to the bright cataclysmic variable.

to 10^{15} cm s^{-2}, adapted to the masses and radii investigated. Finally we use the nsatmos model described by Heinke et al. (2006). This model includes a range of surface gravities and effective temperatures, and incorporates thermal electron conduction and self-irradiation by photons from the compact object. It also assumes negligible (less than 10^9 G) magnetic fields and a pure hydrogen atmosphere.

For each neutron star, we fitted the spectrum obtained from all three cameras simultaneously. However, for the neutron star in M 13 we also included the ROSAT PSPC archival observations of this source in M 13 (Verbunt 2001) as in Gendre et al. (2003b), as the ROSAT data extends below the XMM-Newton data, down to 0.1 keV (only 11.5 ks of data exists in the archives for ω Cen, which is insufficient to improve our spectra. No data exist for NGC 2808). The ROSAT PSPC has a poorer angular resolution than the EPIC cameras (PSPC = 25″ and MOS = 6″) and the spectrum extracted contains data from both the neutron star and the source found at 18.4″ from the neutron star, see Fig. 1. We have extracted the XMM-Newton EPIC MOS spectrum of this source. The best fit to this spectrum is either a power law, $\Gamma=1.75\pm^{0.61}_{0.55}$, Cstatistic = 5.96 (8 bins) or a bremsstrahlung model, $kT=4.49\pm^{171.70}_{2.60}$, Cstatistic = 5.98 (8 bins). This source contributes approximately 28% of the counts in the ROSAT band (0.1-2.4 keV). To take this source into account, we have allowed the normalisation for the ROSAT data to float, to account for the uncertain cross-calibration between the two observatories.

All the data were binned to contain a minimum of 20 counts per bin where possible and we used the χ^2 technique to judge the goodness of the model fits. However, for ω Cen and NGC 2808 the data were binned with 15 counts per bin (to increase the number of data points). In these cases we used the C-statistic to judge the goodness of the fit, as the number of counts per

Table 2: Results of the spectral fitting for the three neutron stars with the three different hydrogen atmosphere models, as described in Section 3.

Cluster	NSA	NSAGRAV	NSATMOS	L_{bol} (erg s^{-1})
ω Cen	N_H=$0.12\pm^{0.04}_{0.02}$	N_H=$0.11\pm^{0.05}_{0.03}$	N_H=$0.12\pm^{0.04}_{0.02}$	4.91×10^{32}
	$log(T)$=$5.99\pm^{0.30}_{0.04}$	$log(T)$=$5.99\pm^{0.20}_{0.11}$	$log(T)$=$5.98\pm^{0.33}_{0.10}$	
	M=$1.76\pm^{0.74p}_{1.26p}$	M=$1.40\pm^{1.1p}_{1.10p}$	M=$1.66\pm^{0.84}_{1.16p}$	
	R=$11.30\pm^{7.27}_{6.30p}$	R=$10.00\pm^{7.80}_{4.00p}$	R=$11.66\pm^{7.03}_{4.99}$	
	Cstat= 91.28, 85 dof	Cstat= 91.26, 85 dof	Cstat= 91.35, 85 dof	
M 13	N_H=$0.013\pm^{0.005}_{0.005}$	N_H=$0.013\pm^{0.005}_{0.004}$	N_H=$0.012\pm^{0.004}_{0.003}$	5.08×10^{32}
	$log(T)$=$6.00\pm^{0.01}_{0.01}$	$log(T)$=$6.00\pm^{0.04}_{0.02}$	$log(T)$=$6.00\pm^{0.01}_{0.09}$	
	M=$1.38\pm^{0.08}_{0.23}$	M=$1.39\pm^{0.51}_{0.67}$	M=$1.30\pm^{0.06}_{0.12}$	
	R=$9.95\pm^{0.24}_{0.27}$	R=$9.95\pm^{2.21}_{0.36}$	R=$9.77\pm^{0.09}_{0.29}$	
	χ^2_ν=1.10, 62 dof	χ^2_ν=1.10, 62 dof	χ^2_ν=1.08, 62 dof	
NGC 2808	N_H=$0.17\pm^{0.05}_{0.09}$	N_H=$0.18\pm^{0.11}_{0.07}$	N_H=$0.16\pm^{0.14}_{0.05}$	1.02×10^{33}
	$log(T)$=$6.04\pm^{0.07}_{0.14}$	$log(T)$=$6.08\pm^{0.06}_{0.17}$	$log(T)$=$6.03\pm^{0.01}_{0.25}$	
	M=$0.67\pm^{0.59}_{0.13}$	M=$0.95\pm^{1.55p}_{0.65p}$	M=$0.91\pm^{1.60}_{0.41p}$	
	R=$8.45\pm^{0.36}_{3.45p}$	R=$7.48\pm^{3.57}_{1.48p}$	R=$6.10\pm^{11.47}_{1.10p}$	
	Cstat=17.59, 19 dof	Cstat=18.12, 19 dof	Cstat=16.95, 19 dof	

The column density, N_H is $\times 10^{22}$ cm^{-2}, the temperature (T) is given as the logarithm of the temperature in Kelvin, the masses are in solar units and the radii in kilometres. All errors are given at the 90% confidence limit for the one interesting parameter. To calculate the errors, the mass and distance were held fixed and all other parameters were allowed to vary, except when calculating the error on the mass, when the radius was held fixed. A 'p' after the error value indicates that the hard limit of the model was reached. The estimated unabsorbed bolometric luminosity for each neutron star is also given.

bin is no longer strictly in the Gaussian statistics regime but approaches that of the Poissonian statistics regime. Even though we are at the limit between the two regimes, the C-statistic has been shown to work well at even higher counts (Nousek & Shue 1989) and should therefore give good results. The inverse is not necessarily true. Nousek & Shue (1989) showed that using the Levenberg-Marquardt algorithm (the algorithm used in Xspec) for small numbers of events per bin gives a systematic bias.

3.1. Absorption in the spectra

For each model we included (photoelectric) absorption along the line of sight to the object. This was initially fixed at the value determined for each cluster (see Table 1) and then allowed to vary. In every case we found that we required additional absorbing material, assumed to be additional gas intrinsic to the system. This was typically 30-60% more i.e. ω Cen required an $n_H \sim 0.11 \times 10^{22}$ cm^{-2}, an increase of 60% with a ftest probability of 0.0099, indicating that it is reasonable to include additional material. The normalisation was fixed to the value corresponding to the distance to the cluster (see Table 1) and the masses and radii were initially frozen to 1.4 $M_\odot$ and 10.0 km, but then allowed to vary.

We then tried to constrain the nature of the additional absorbing material, in the same way as Heinke et al. (2006), by employing the *Xspec* model *vphabs* and using the abundances corresponding to those of each of the clusters. For M 13 we chose the iron abundance to be 3% solar ([Fe/H] = -1.5), the abundances of C, N and O to be 5% solar ([X/H] = -1.32), the abundances of Ne to Ca to be 4% solar ([X/H] = -1.38) and that of helium to be of solar abundance, following Cohen & Melendez (2005). For ω Cen the situation is more complicated as there are three distinct populations of stars in this cluster, see e.g. Origlia et al. (2003). We elected the abundances from the largest population in the cluster, basing our choice on the fact that the highest probability was that the donor star comes from the largest population. We adopt the iron abundance to be 3% solar ([Fe/H] = -1.58), the abundances of C, N and O to be 6% solar ([X/H] = -1.24), the abundances of

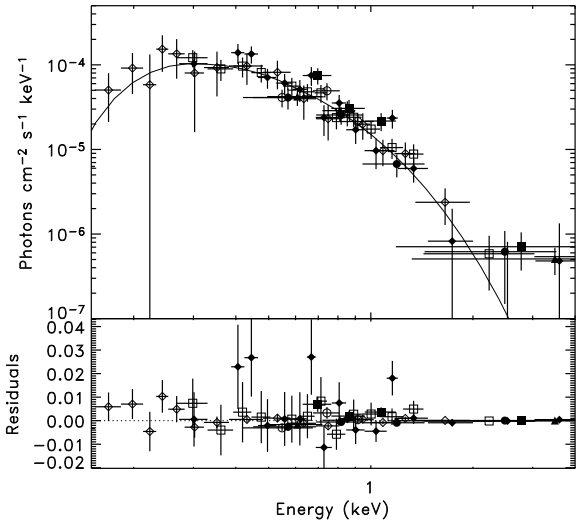

Fig. 3.— Unfolded spectrum of the neutron star in M 13 with the best nsatmos model fit and the residuals to the fit. The different symbols indicate the data from the different instruments used: open diamonds show PSPC data, filled circles and triangles show MOS 1 data, filled squares and empty circles show MOS 2 data and filled diamonds and empty squares show pn data.

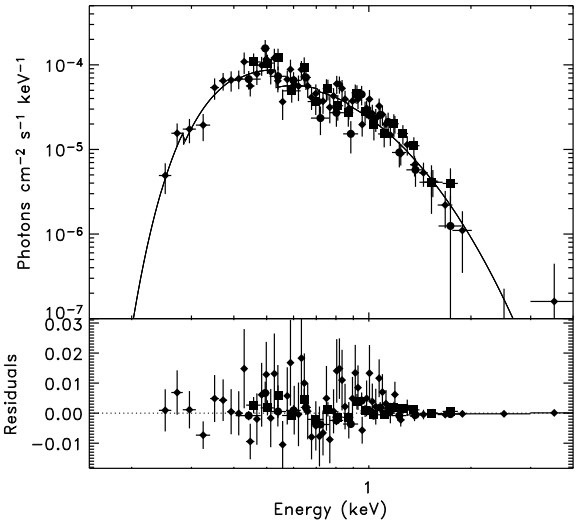

Fig. 4.— Unfolded spectrum of the neutron star in ω Cen with the best nsatmos model fit and the residuals to the fit. The different symbols indicate the data from the different instruments used: filled circles show MOS 1 data, filled squares show MOS 2 data and filled diamonds show pn data.

Ne to Ca to be 6% solar ([X/H] = -1.19) and again that of helium to be of solar abundance, following Origlia et al. (2003) and Norris (2004). For NGC 2808 we select the iron abundance to be 9% solar ([Fe/H] = -1.06), the abundances of C, N and O to be 32% solar ([X/H] = -0.5), the abundances of Ne to Ca to be 16% solar ([X/H] = -0.8) and that of helium to be of solar abundance, following Castellani et al. (2006) and Gratton (1982). Again, however, it is believed that NGC 2808 has as many as three populations of stars, with different abundances (Piotto et al. 2007). We chose the abundances for the only population with sufficient information in the literature. We then modelled the neutron star spectra fixing the photoelectric absorption (phabs) to be that of the cluster and allowing the photoelectric absorption with variable abundances (vphabs) to vary (using the abundances given above). The results that we obtained gave very small masses and/or radii, often small enough to hit the lower mass or radius limit allowed in the models (see below for values).

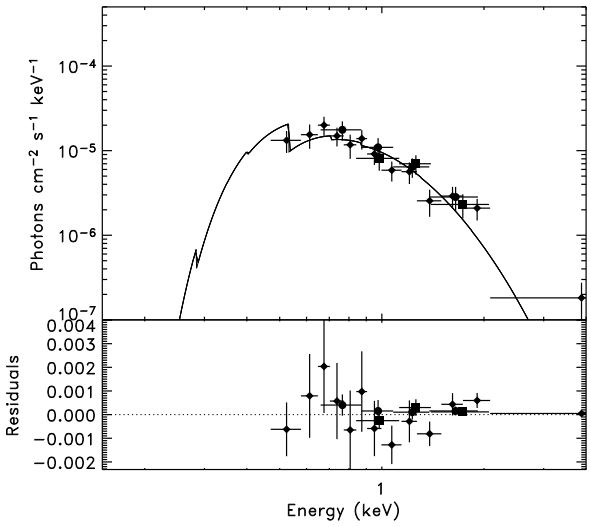

Fig. 5.— Unfolded spectrum of the neutron star in NGC 2808 with the best nsatmos model fit and the residuals to the fit. The different symbols used are the same as those employed in Fig. 4.

We thus decided to determine whether our data are of sufficiently good quality to constrain the na-

ture of the additional absorbing material. We simulated a spectrum similar to that obtained for ω Cen, using the simple phabs model. We modelled this spectrum in *Xspec* using first the phabs model and then the vphabs model. We obtained similar χ^2_ν values (1.17, 78 dof when using phabs and 1.29, 78 dof when using vphabs), but again the masses and radii were very low when the vphabs model was employed, only $\sim$80% of the value given to simulate the spectrum as opposed to values within 10% when using the phabs model. We also simulated the same spectrum but using the vphabs model. Again, modelling this spectrum in Xspec using the vphabs model we found values as low as 33% of the original value, yet when modelling with the phabs model our values are within 5% of our original values. Further, we obtain equally good fits using vphabs to our simulated spectrum (χ^2_ν=1.09, 78 dof) when we choose abundances that are different by 300% to those used in the simulated spectrum, and we still have the problem that either the mass or the radius is very small. We therefore conclude that the quality of our data is insufficient to constrain the nature of the additional absorbing material and we use the phabs model only.

3.2. Contribution from neighbouring sources

We also investigated whether we required an extra power law tail, especially for the two neutron stars found in proximity of other sources i.e. the neutron stars in M 13 and NGC 2808. This is important as substantial flux from other sources is likely to be the dominant source of counts in the higher energy bands (i.e. above 1 keV). This may tend to systematically bias the spectral fits to higher temperatures, and thus smaller radii.

To do this we extracted the spectra of the neighbouring sources and determined their photon indices ($\Gamma\sim$1.75 for M 13 and $\Gamma\sim$1.5 for NGC 2808). We then estimated the contribution from the neighbouring sources in the extraction region for each neutron star (8% for M 13 and 20% for NGC 2808, see Figs 1 and 2). We used these values and refitted our spectra. Interestingly, we found values very similar to those obtained when no power law was included. Even allowing the normalisation to increase, increasing the weight of the power law, made little difference to the fits. Ftests show that adding the power law is not necessary. Probability results for fitting nsa, nsatmos and nsagrav models with and without the additional power laws to the neutron star in M 13 are 0.31, 0.22 and 0.199 respectively and to the neutron star in NGC 2808 are 0.13, 0.06 and 0.08 respectively. We therefore conclude that adding a power law is not required by the data.

The spectra of the three neutron stars can be found in Figs. 3-5, along with the best fitting nsatmos model.

3.3. Modelling the spectra

The principal goal of our spectral fitting is to self-consistently constrain the allowed space in mass and radius using our three neutron stars, but also to test the reliability and accuracy of the three models examined. Table 2 gives the best fits for each neutron star fitted with each of the three models, along with the best fitting values for the column densities, surface temperatures of the neutron stars, masses and radii. Errors are also given at the 90% confidence limit for the one interesting parameter. To calculate the errors, the mass and distance were held fixed and all other parameters were allowed to vary, except when calculating the error on the mass, when the radius was held fixed instead of the mass. We also give the estimated bolometric luminosity of the neutron star. We found that we did not require any additional parameters, such as lines or edges to fit these data. However, this may be due to the quality of the data, where deeper observations may reveal spectral features that will be useful to constrain the gravitational redshift at the NS surface (Brown, Bildsten & Rutledge 1998; Rutledge et al. 2002; Heinke et al. 2003).

We use the steppar command in XSPEC to vary both the radius and mass parameters simultaneously, allowing the temperature to vary as well to find the best fit. The minimum (and maximum) radii allowed with these models are 5 km (30/20 km) for the nsatmos and nsa models respectively and 6 km (20 km) for the nsagrav model. We chose an inferior limit of 8 km and a superior limit of 18 km as all three models gave stable results when fitting the data in these regions. The minimum (and maximum) masses allowed with these models are $0.5M_\odot$ ($3.0/2.5M_\odot$) for the nsatmos and nsa models respectively and $0.3M_\odot$ ($2.5M_\odot$) for the nsagrav model. We chose the region be-

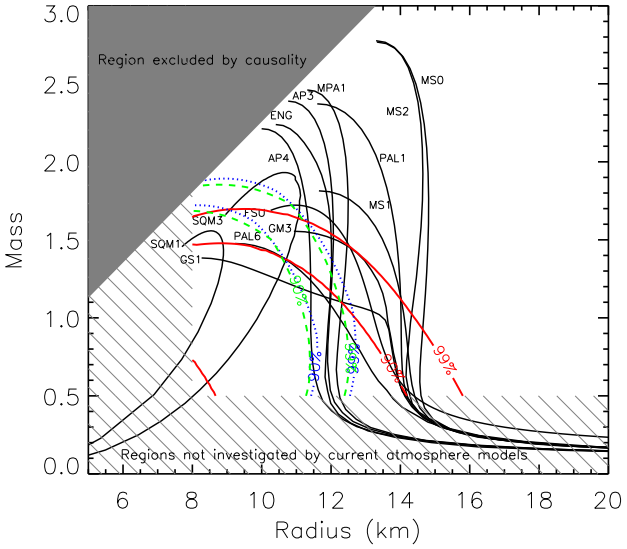

Fig. 6.— Contour plot showing the results of modelling the neutron star in M 13 with the xspec models: nsa (solid/red line), nsatmos (dotted/blue line) and the nsagrav (dashed/green line). The 90% and 99% confidence contours for the neutron star masses ($M_\odot$) and the radii (km) are plotted along with neutron star equations of state taken from Lattimer & Prakash (2007)

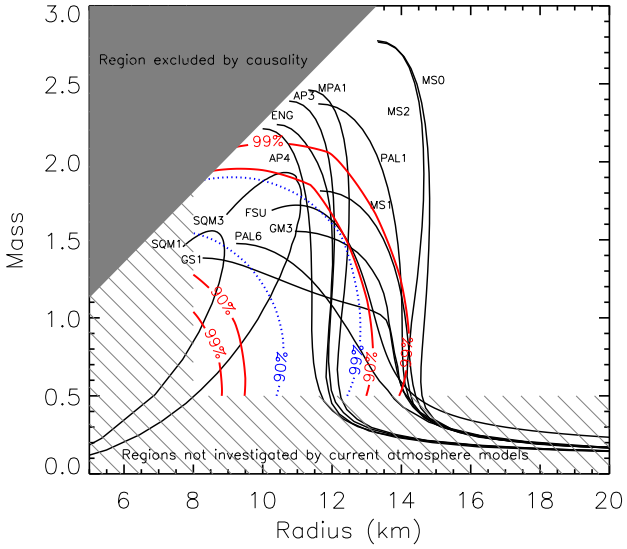

Fig. 7.— Contour plot showing the results of modelling the neutron stars in ω Cen (solid/red line) and NGC 2808 (dotted/blue line) with the xspec model nsatmos. The 90% and 99% confidence contours for the neutron star masses ($M_\odot$) and the radii (km) are plotted along with neutron star equations of state taken from Lattimer & Prakash (2007)

tween 0.5 and 2.3$M_\odot$ as again all three models gave stable results in these regions. We show 90% confidence, and 99% confidence ($\Delta\chi^2 = 4.61$, and 9.21 respectively) contours in neutron star mass and radius. Fig. 6 shows the results of modelling the neutron star in M 13 with all three neutron star atmosphere models. This figure indicates that the two models, nsatmos and nsagrav, give comparable results, whereas the nsa model gives differing results. The nsa model is more accurate in constraining R_∞ than the nsatmos and nsagrav models, due to a degeneracy in spectral shape variations between the surface gravity and the surface temperature. However, here we calculate a range of neutron star masses and radii, for which the nsatmos and nsagrav, thanks to their variable surface gravities, are better adapted (see the discussion in Heinke et al. 2006). The use of these fixed gravity models for testing neutron stars with a variety of masses and radii (and therefore gravities) is not therefore strictly appropriate. This is borne out by the modelling. For this reason and to simplify the following plots, we ignore the nsa model (as it is less accurate) and we plot only the nsatmos model (as the nsagrav and nsatmos models are similar) to show the constraints on mass and radius determined by modelling ω Cen and NGC 2808 (Fig. 7). The loci of models for the equations of state for dense matter are those described in Lattimer & Prakash (2007) and Lattimer & Prakash (2001) which include diverse equations such as: SQM - Prakash, Cooke & Lattimer (1995), a Strange Quark Matter model, PAL - Prakash, Ainsworth & Lattimer (1988) a neutron and proton model using a schematic potential, GM - Glendenning & Moszkowski (1991), a model containing neutrons, protons and hyperons using a field theoretical approach, GS - Glendenning & Schaffner-Bielich (1999), a model containing neutrons, protons and kaons using a field theoretical approach.

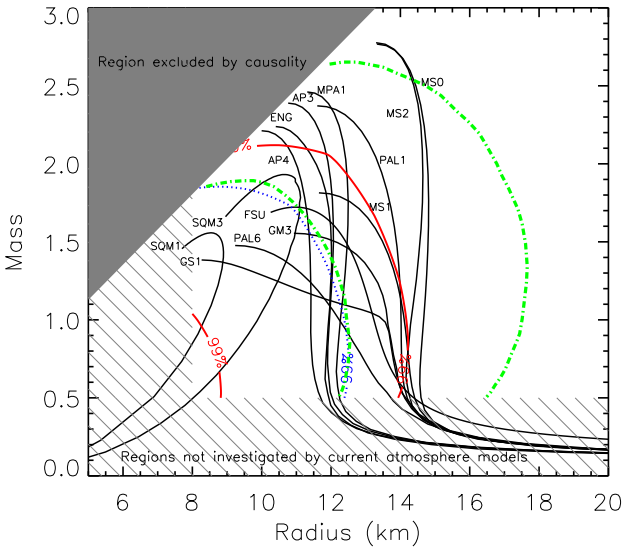

Fig. 8.— Contour plot showing the results of modelling the neutron stars in M 13 (dotted/blue line), ω Cen (solid/red line) and X7 in 47 Tuc (dashed-dotted/green line) (Heinke et al. 2006) with the xspec model nsatmos. The 99% confidence contours for the neutron star masses ($M_\odot$) and the radii (km) are plotted along with neutron star equations of state taken from Lattimer & Prakash (2007). The grey hashed region indicates the region not investigated with the models.

4. Discussion and Conclusions

As seen in Section 3 even if the nsa model is more accurate in constraining R_∞ than the nsatmos and nsagrav models, when calculating a range of neutron star masses and radii, we find that the nsatmos and nsagrav models are better adapted. We conclude that the use of fixed gravity models for testing neutron stars with a variety of masses and radii (and therefore gravities) is not strictly appropriate as previously indicated by Gänsicke et al. (2002) and Heinke et al. (2006).

Using the results from Figs. 6 and 7, and the results found by Heinke et al. (2006) when fitting Chandra observations of X7 in 47 Tuc, we show the allowed equations of state in Fig. 8. Modelling the neutron star in M 13 alone shows that the data do not favour the stiffer equations of state, such as MS0-2 and PAL 1. We combine these results with those from modelling the neutron star in ω Cen. The low quality data for the neutron star in NGC 2808 results in very poor constraints for this object and hence we disregard this source in the discussion, although the results seem to be similar to those for the neutron star in M 13. The equations of state that are satisfied by all three neutron stars fall in the middle of the diagram and includes the equations of state of normal nucleonic matter and one strange quark matter model. The equations allowed are GS1, PAL 6, AP3 & 4, GM3, FSU, SQM3, ENG and MPA1, with radii above 8 km and masses up to 2.4 $M_\odot$.

This article was based on observations obtained with XMM-Newton, an ESA science mission with instruments and contributions directly funded by ESA Member States and NASA. The authors thank J. Lattimer for providing them with the mass-radius relationships for the different equations of state shown in Figures 6-8 and B. Gendre for help with the ROSAT spectrum. The authors also acknowledge the CNES for its support in this research and thank the (anonymous) referee for very valuable comments that have enabled us to improve the quality of this paper.

REFERENCES

Arnaud, K.A., 1996, Astronomical Data Analysis Software and Systems V, eds. Jacoby G. and Barnes J., p17, ASP Conf. Series volume 101

Barret, D., Olive, J.-F., & Miller, M. C. 2005, MNRAS, 361, 855

Brown, E. F., Bildsten, L., & Rutledge, R. E. 1998, ApJ, 504, L95

Castellani, V., Iannicola, G., Bono, G., Zoccali, M., Cassisi, S., & Buonanno, R. 2006, A&A, 446, 569

Cohen, J. G., & Meléndez, J. 2005, AJ, 129, 303

Cottam, J., Paerels, F., & Mendez, M. 2002, Nature, 420, 51

Ehle, M. and the XMM-Newton consortium 2006, XMM-Newton User's Handbook, v. 2.4, Eds. M. Ehle, M. Breitfellner, R. González Riestra, M. Guainazzi, N. Loiseau, P. Rodríguez, M. Santos-Lleó, N. Schartel, L. Tomás, E. Verdugo, M. Dahlem

Ehle, M., Pollock, A.M.T., Talavera, A., Gabriel, C., Chen, B., Ballet, J., Dennerl, K., Freyberg, M., Guainazzi, M., Kirsch, M., Metcalfe, L., Ojero, E., Osborne, J., Pietsch, W., Saxton, R., Smith, M., Verdugo, E 2006b,User's Guide to the XMM-Newton Science Analysis System, v. 4.0, Ed. N. Loiseau

Faulkner, A. J., Kramer, M., Lyne, A. G., & et al. 2005, ApJ, 618, L119

Gänsicke, B. T., Braje, T. M., & Romani, R. W. 2002, A&A, 386, 1001

Gendre, B., Barret, D., & Webb, N.A. 2003a, A&A, 400, 521

Gendre, B., Barret, D., & Webb, N.A. 2003b, A&A, 403, L11

Glendenning, N.K., & Moszkowski, S.K. 1991, Phys. Rev. Lett., 57, 2414

Glendenning, N.K., & Schaffner-Bielich, J. 1999, Phys. Rev., 57, C60, 025803

Gratton, R.G. 1982, A&A, 115, 171

Harris W. E., 1999, Ap&SS, 267, 95, rev. (2003)

Heinke, C. O., Grindlay, J. E., Lloyd, D. A., & Edmonds, P. D. 2003, ApJ, 588, 452

Heinke, C.O., Rybicki, G.B., Narayan, R., & Grindlay, J.E. 2006, ApJ, 644, 1090

Kirsch, M., and the EPIC Consortium, 2002, XMM-SOC-CAL-TN-0018

Lattimer, J.M., & Prakash, M. 2007, PhR, 442, 109

Lattimer, J.M., & Prakash, M. 2001, ApJ, 550, 426

Nice, D. J., Splaver, E. M., Stairs, I. H., Löhmer, O., Jessner, A., Kramer, M., Cordes, J. M. 2005, ApJ, 634, 1242

Norris, J. E. 2004, ApJ, 612, 25

Nousek, J. A., & Shue, D. R. 1989, ApJ, 342, 1207

Origlia, L., Ferraro, F. R., Bellazzini, M., & Pancino, E. 2003, ApJ, 591, 916

Özel, F 2006, Nature, 441, 1115

Piotto, G., Bedin, L. R., Anderson, J., King, I. R., Cassisi, S., Milone, A. P., Villanova, S., Pietrinferni, A., & Renzini, A. 2007, ApJ, 661, 53

Prakash, M., Cooke, J. R., & Lattimer, J. M. 1995, PhRvD, 52, 661

Prakash, M., Ainsworth, T.L., & Lattimer, J. M. 1995, PhRvL, 61, 2518

Predehl, P., & Schmitt, J. H. M. M. 1995, A&A, 293, 889

Rutledge, R. E., Bildsten, L., Brown, E. F., Pavlov, G. G., & Zavlin, V. E. 1999, ApJ, 514, 945

Rutledge, R. E., Bildsten, L. Brown, E. F., Pavlov, G. G., & Zavlin, V. E. 2002, ApJ, 578, 405

Servillat, M., Webb, N.A., & Barret, D. 2007 A&A, submitted

Van Paradijs J., Verbunt F., Shafer R. A., & Arnaud K. A. 1987, A&A, 182, 47

Verbunt, F. 2001, A&A, 368, 137

Webb, N.A., Serre, D., Gendre, B., Barret, D., Lasota, & J.-P., Rizzi, L. 2004, A&A, 424, 133

Webb, N.A., Wheatley, P.J., & Barret, D. 2006, A&A, 445, 155

Weisberg, J.M., & Taylor, J.H. 2005, ASPC, 328, 25

Zavlin, V.E., Pavlov, G.G., & Shibanov, Yu.A. 1996, A&A, 315, 141

This 2-column preprint was prepared with the AAS LaTeX macros v5.2.